Author(s): Broas, Mikael; Sippola, Perttu; Sajavaara, Timo; Vuorinen, Vesa; Perros, Alexander Pyymaki; Lipsanen, Harri; Paulasto-Kröckel, Mervi

Title: Structural and chemical analysis of annealed plasma-enhanced atomic layer deposition aluminum nitride films

Year: 2016

Version:

Please cite the original version:

Broas, M., Sippola, P., Sajavaara, T., Vuorinen, V., Perros, A. P., Lipsanen, H., & Paulasto-Kröckel, M. (2016). Structural and chemical analysis of annealed plasma-enhanced atomic layer deposition aluminum nitride films. Journal of Vacuum Science and Technology A, 34(4), Article 041506. https://doi.org/10.1116/1.4953029

JVSTA Journal of Vacuum Science & Technology A

Structural and chemical analysis of annealed plasma-enhanced atomic layer deposition aluminum nitride films

Mikael Broas, Perttu Sippola, Timo Sajavaara, Vesa Vuorinen, Alexander Pyymaki Perros, Harri Lipsanen, and Mervi Paulasto-Kröckel

Citation: Journal of Vacuum Science & Technology A **34**, 041506 (2016); doi: 10.1116/1.4953029
View online: http://dx.doi.org/10.1116/1.4953029
View Table of Contents: http://scitation.aip.org/content/avs/journal/jvsta/34/4?ver=pdfcov
Published by the AVS: Science & Technology of Materials, Interfaces, and Processing

Structural and chemical analysis of annealed plasma-enhanced atomic layer deposition aluminum nitride films

Mikael Broas[a),b)]
Department of Electrical Engineering and Automation, Aalto University, P.O. Box 13500, FIN-00076 Aalto, Espoo, Finland

Perttu Sippola[a)]
Department of Micro- and Nanosciences, Aalto University, P.O. Box 13500, FIN-00076 Aalto, Espoo, Finland

Timo Sajavaara
Department of Physics, University of Jyväskylä, P.O. Box 35, FIN-40014 Jyväskylä, Finland

Vesa Vuorinen
Department of Electrical Engineering and Automation, Aalto University, P.O. Box 13500, FIN-00076 Aalto, Espoo, Finland

Alexander Pyymaki Perros and Harri Lipsanen
Department of Micro- and Nanosciences, Aalto University, P.O. Box 13500, FIN-00076 Aalto, Espoo, Finland

Mervi Paulasto-Kröckel
Department of Electrical Engineering and Automation, Aalto University. P.O. Box 13500, FIN-00076 Aalto, Espoo, Finland

(Received 11 February 2016; accepted 16 May 2016; published 3 June 2016)

Plasma-enhanced atomic layer deposition was utilized to grow aluminum nitride (AlN) films on Si from trimethylaluminum and N_2:H_2 plasma at 200 °C. Thermal treatments were then applied on the films which caused changes in their chemical composition and nanostructure. These changes were observed to manifest in the refractive indices and densities of the films. The AlN films were identified to contain light element impurities, namely, H, C, and excess N due to nonideal precursor reactions. Oxygen contamination was also identified in the films. Many of the embedded impurities became volatile in the elevated annealing temperatures. Most notably, high amounts of H were observed to desorb from the AlN films. Furthermore, dinitrogen triple bonds were identified with infrared spectroscopy in the films. The triple bonds broke after annealing at 1000 °C for 1 h which likely caused enhanced hydrolysis of the films. The nanostructure of the films was identified to be amorphous in the as-deposited state and to become nanocrystalline after 1 h of annealing at 1000 °C. © *2016 American Vacuum Society*. [http://dx.doi.org/10.1116/1.4953029]

I. INTRODUCTION

Aluminum nitride (AlN) is utilized in various electronics and sensor applications. For example, it is used in ceramic substrates in high power integrated circuits (IC),[1] resonator applications,[2] and light emitting diodes (LED).[3] All of these applications take advantage of the excellent thermal and/or electrical properties of AlN. Specifically, ceramic substrates for power ICs utilize the high thermal conductivity and mechanical rigidity of AlN.[4] Resonator applications exploit the piezoelectricity of crystalline AlN together with its dielectric properties.[5] Finally, some LEDs utilize AlN as a strain buffer and nucleation material between Si substrates and subsequent GaN layers,[6] and as a part of active photon emitting structures down to the UV range.[7]

AlN can be fabricated by various methods including "bulk material fabrication" methods, such as carbothermal nitridation of Al_2O_3 and subsequent sintering,[8,9] or by thin film deposition methods such as sputtering[10] or metalorganic chemical vapor deposition.[11] More recently, plasma-enhanced atomic layer deposition (PEALD) has been demonstrated as an alternative method for AlN deposition.[12–22] The AlN process is also available for thermal ALD but in that case the source material selection is limited and above 400 °C deposition temperatures are required.[15] In contrast, the attractive properties of PEALD films include low temperature processing (typically below 300 °C), thus increasing the choice of precursors and materials, enabling tunable material properties, and still allowing the typical ALD thickness control below 1 nm accuracy.[23] For instance, varying the ratio of the N_2:H_2 plasma precursor could offer opportunities in controlling AlN properties. Previous research shows that PEALD AlN films could be polycrystalline[12] or amorphous[15] around 200 °C deposition temperature. Furthermore, the deposited films typically contain high amounts of hydrogen ranging up to 20 at. %. Other impurities can also be present due to nonideal precursor reactions and imperfect isolation of the reaction chamber from the ambient.[22] Some of the incorporated impurities are volatile in higher temperatures causing instability of the films due to outgassing or increased chemical reactivity of the AlN, which in turn would cause deterioration in the performance of the final application. Moreover, the impurities can also be connected to the crystallinity of the films.[24]

[a)]M. Broas and P. Sippola contributed equally to this work.
[b)]Electronic mail: mikael.broas@aalto.fi

The stability and oxidation of AlN produced via the more-established methods have been studied: Lin *et al.*[25] studied the oxidation behavior of sputtered AlN in various atmospheres (air, nitrogen gas with $\sim 10^{-5}$ atm O_2 partial pressure, and forming gas with $\ll 10^{-5}$ atm O_2 partial pressure) between 700 and 1200 °C. They concluded that the oxidation of the films started at 900 °C in air and was shifted to above 1000 °C in a nitrogen-rich environment. The films became completely oxidized, composed of rhombohedral α-Al_2O_3, after two hours of annealing at 1100 °C when the annealing atmosphere was air, but were only partially oxidized at 1200 °C when using the forming gas. Similar results have been reported by Ansart *et al.*[26] who concluded that no chemical alterations of AlN deposited with plasma-enhanced CVD took place below 850 °C in air and that transformation to α-Al_2O_3 took place rapidly above 1100 °C in air. Dalmau *et al.*[27] reported AlN to form a thin layer ($\sim$1 nm) of AlOOH at room temperature under ambient-air exposure. This layer then approached the stoichiometry of Al_2O_3 when annealed under vacuum in higher temperatures. Furthermore, Wang *et al.*[28] have shown the hydrogen content of sputtered AlN films to affect the hydrolysis of the films under ambient-air storage.

In contrast to the more established thin film deposition methods, little is known on the annealing behavior of PEALD AlN films. Especially of interest are how the impurities of PEALD AlN films behave at higher temperatures, and how the impurities affect the structure of the films. The scope of this paper is thus to investigate the changes in the chemical composition and structure of PEALD AlN films when they undergo thermal treatments. The analysis is further correlated with various AlN film properties—refractive index, density, and thermal stability (in the form of thickness change). The results may be utilized in improving the material quality of the as-deposited films, in predicting reliability in demanding environments, and optimizing other manufacturing processes that could take place after the AlN deposition.

II. EXPERIMENT

A. ALD setup and annealing

Aluminum nitride films were deposited on (100) silicon wafers with native oxides in a Picosun R-200 ALD reactor with a remote inductively coupled plasma configuration at a base pressure of 2 hPa (2 mbar). A loadlock connected to a cluster tool was used to deliver the substrates into the reactor chamber in order to reduce the amount of ambient impurities, especially water vapor (later, a minor leak in the water line valve was found which introduced some ambient air impurities to the films). Trimethylaluminum (TMA) ($\geq$98% purity) and N_2:H_2 plasma radicals were used as the precursors while the carrier and purge gases were Ar and N_2. The TMA source was kept at 23 °C. The deposition temperature was fixed at 200 °C and plasma power to 2500 W for all of the PEALD runs.

The PEALD runs were completed with two differing plasma flow ratios. In the case of a 1:1 N_2:H_2 flow ratio, the flow rates for TMA and N_2:H_2 were set to 150 and 45:45 sccm, while in a 3:1 N_2:H_2 case those were 130 and 75:25 sccm. In addition, the N_2 and Ar carrier gas flows from the metal precursor lines and plasma gas lines were 40 and 100 sccm, respectively, during the runs.

The saturated, self-terminating film growth of the 1:1 flow ratio sample was achieved with TMA and N_2:H_2 pulse/purges which, respectively, were 0.1/6 and 13/2 s, producing a growth-per-cycle (GPC) of 0.63 Å/cycle on a 150 mm Si wafer. In the case of the 3:1 flow ratio, the precursor pulse/purges were 0.1/6 and 10.5/3 s, respectively, with a GPC of 0.64 Å/cycle on a 100 mm Si wafer. The actual plasma exposure time was 12 s in the first case and 8 s in the latter.

The AlN films were annealed for 1 h at soak temperatures of 400, 600, 800, and 1000 °C in high vacuum (HV) conditions ($p_{tot} < 10^{-6}$ mbar) in a furnace (Webb Red Devil M). The ramp rate used in the experiments was approximately 16 K/min. The vacuum turbomolecular pump had a pumping speed of 240 l/s, and the chamber had a volume of approximately 15 l. The nominal vacuum gauge operation range was reported to be from 10^{-7} mbar to 1 atm. The chemical stability of AlN is especially affected by the partial pressures of oxygen and nitrogen. The manufacturer provided data of the residual gases in the range of 0–90 amu at 1200 °C during stable high vacuum conditions. According to the data, the residual oxygen partial pressure inside the chamber is clearly below 10^{-7} mbar.

B. Thin film characterization

An ellipsometer (Plasmos SD 2300) was used to measure the thicknesses and refractive indices of the thin films. The ellipsometer utilized 632.8 nm He-Ne laser as the light source while the angle of incidence was fixed to 70°. The thickness and refractive index values were determined from the measured optical parameters and initially assumed values by the ellipsometer software using automatic iterative data fitting method based on a one-layer AlN-on-Si model.

X-ray reflectivity (XRR) and x-ray diffraction (XRD) analyses were carried out with an x-ray diffractometer (Philips X'Pert Pro) utilizing the Cu $K_{\alpha 1}$ radiation. XRR was employed in measuring the density and XRD in defining the crystallinity of the PEALD AlN films. The measured XRR curves were fitted using Parratt's formalism to extract the density of the films. An in-house developed software was used to find the best fit.[29] All fits were done on a one-layer model in order to capture the average changes in the densities. XRD was conducted in the Bragg–Brentano geometry scanning over a broad range of the θ-2θ of the typical reflections in the AlN-Al_2O_3 systems. The structure and crystallinity were also further studied by preparing cross-sectional transmission electron microscopy (TEM) samples. The preparation was performed either by using a focused ion beam (FEI Helios NanoLab 600 FIB) system or by mechanical polishing and ion milling. TEM studies were conducted either at 300 kV with an image C_s-corrected FEI Titan^3 G2 60–300 TEM or at 200 kV with a FEI Tecnai F20-FEGTEM S-Twin TEM. Evaluation of the crystallinity was based on

visual inspection of the high resolution TEM (HRTEM) images and fast Fourier transform (FFT) images.

Film composition analyses were carried out with time-of-flight elastic recoil detection analysis (ToF-ERDA, University of Jyväskylä[30]) and Fourier transform infrared (FTIR) spectroscopy. ToF-ERDA measurements with 13.6 MeV $^{63}Cu^{7+}$ ions were utilized in obtaining quantitative information of the films' elemental composition, including hydrogen concentration. However, ToF-ERDA does not give information on the chemical binding states of the elements. For example, it is not possible to differentiate between solute hydrogen and hydrogen in different hydroxide species. FTIR was thus used to evaluate the possible chemical compounds in the film. The FTIR analyses were conducted with a Thermo Electron Corporation Nicolet 380 FTIR spectrometer. The measurements were conducted by collecting a background with 64 scans after which the actual scans were collected with 128 scans. All of the scans were conducted on wavenumbers 400–4000 cm^{-1}. The resolution was 4 cm^{-1}. After each measurement, the background was removed from the scans.

Finally, thermal desorption spectroscopy (TDS) was briefly utilized to confirm hydrogen desorption from one of the films. This was done in order to validate the system, which has been more extensively used for bulk metallic samples, for future thin film research. The TDS apparatus is presented in detail in Ref. 31. Briefly, the system consists of an ultrahigh vacuum (UHV) chamber equipped with a small vacuum furnace and an air-lock vacuum chamber for specimen supply. The pumping system has an effective pumping rate of 6.6×10^{-2} m^3/s. A personal computer using LAB VIEW based software is used for controlling a mass spectrometer unit and the furnace heating rate. The basic vacuum in the UHV chamber is kept at a level of 7×10^{-9} mbar. The heating system provides direct control of the specimen temperature in the temperature range from room temperature to 1000 °C with a heating rate from 1 to 10 K/min.

III. RESULTS AND DISCUSSION

A. Refractive index, density, and thickness

The evolution of the refractive indices, densities, and thicknesses of the two sample types (i.e., 1:1 and 3:1 N_2:H_2 flow) were studied as a function of the annealing temperature. The original thicknesses and nonuniformities for the 1:1 flow sample were 84 nm and 2.2%, and for the 3:1 sample 53 nm and 1.4% (nine measurements on the 100 mm wafer and 15 measurements on the 150 mm wafer). Figures 1 and 2 present the XRR density and the ellipsometer refractive index measurements. The values represent average values of the whole films (i.e., one-layer models). The error bars in the density calculations represent the uncertainty associated with fitting the simulated curves to the measurements. For refractive index, the error bars are ±1 standard deviation (±1 σ). Each annealed refractive index data point consists of two measurements conducted on four or more 1 × 1 cm chips. Both graphs depict the decrease in the density of the films initially, after which the density starts to increase surpassing the initial density when annealed at 1000 °C. In contrast, the refractive index of the 1:1 N_2:H_2 films monotonically decreases, whereas in the 3:1 sample, the changes in the refractive index are less pronounced with a slight increase toward 1000 °C.

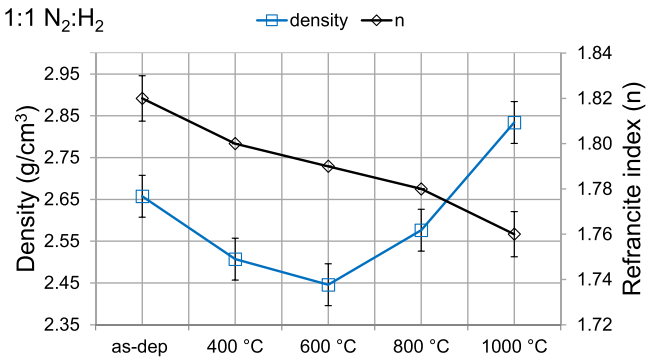

FIG. 1. (Color online) Development of density and refractive index as a function of annealing temperature for 1:1 N_2:H_2 gas flow AlN films.

Both the refractive index and the density of the samples are lower than the values for bulk AlN (~2.1 and 3.25 g/cm^3, respectively).[32] This behavior is expected for thin films which might not be completely crystalline (less dense packing) and have various impurities. The magnitude of the refractive index is mainly dictated by the density and the polarizability of the ions.[33] Therefore, if no material changes take place (i.e., no change in polarizability), a higher density would lead to a higher refractive index. Indeed, the 3:1 N_2:H_2 flow samples display such a straightforward relation; the changes in the refractive index follow the changes in the density. The 1:1 N_2:H_2 samples initially follow this pattern; both the refractive index and the density decrease until the 600 °C anneal. After 800 and 1000 °C thermal treatments, the density of the 1:1 N_2:H_2 samples increases notably while the refractive index further decreases. This implies that the polarizability of the ions decreases, which in turn implies chemical or structural changes in the thin film. For example, α-Al_2O_3 (corundum phase) has a higher density but a lower refractive index than wurtzite AlN. Al_2O_3 is also more stable than AlN at higher temperatures. The initial decrease in the density of the samples is likely due to outgassing of volatile products that are embedded in the films due to nonideal

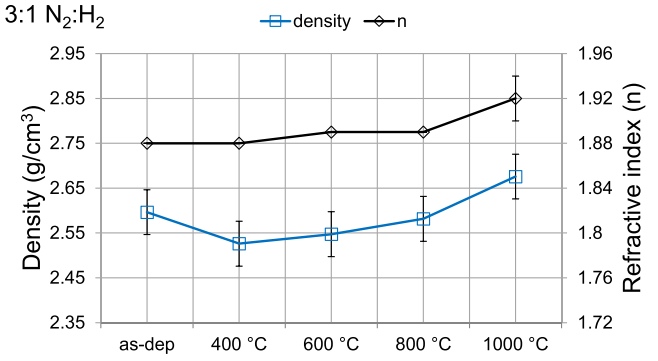

FIG. 2. (Color online) Development of density and refractive index as a function of annealing temperature for 3:1 N_2:H_2 gas flow AlN films.

precursor reactions. The densification at the higher annealing temperatures may be related to crystallization phenomena or chemical changes (e.g., alumina formation) in the films. On the contrary, the refractive index and density behavior of the 3:1 N_2:H_2 film is more stable during the thermal treatments. Therefore, the as-deposited structure is closer to the higher temperature stable structure such as alumina.

The thicknesses of the films were also observed to change due to the annealing treatments (Fig. 3). Two dies per each thermal treatment were measured with the ellipsometer. The dies were from random parts of the wafers, i.e., the original thicknesses had minor deviations from die to die due to the nonuniformity of the deposited AlN films. Therefore, Fig. 3 presents the average change in the thickness of two dies due to respective annealing treatments. The original thicknesses of the films were not considered to markedly affect the thickness change, i.e., surface layers were mainly considered to participate in evaporation. Furthermore, the films were thought to be thick enough to have enough species that could react by either diffusing to the surface or reacting with gaseous species diffusing into the film from the annealing chamber before the annealing stopped, i.e., the films not reaching thermodynamic equilibrium.

Both of the AlN films have similar thickness decrease after annealing up to 800 °C, indicating that the evaporating species are the same in both films. The density changes play a role also in the thicknesses of the films, and the total process is not straightforward to interpret. Nevertheless, the changes in the thicknesses of the films are not negligible. Such behavior would potentially affect the performance of a device relying on precise thickness-property tailoring. In 1000 °C, the 3:1 N_2:H_2 AlN film further decreases in thickness following almost a linear relationship. However, the decrease in the thickness of the 1:1 N_2:H_2 AlN film is close to that of annealing in 400 °C after the 1000 °C anneal. Therefore, the assumption of having enough species in the film for constant mass transport to the surface may not be accurate anymore.

B. Composition and structure

The composition and microstructure of the PEALD AlN films were analyzed in the as-deposited state and after the thermal treatments. The analyses were conducted utilizing

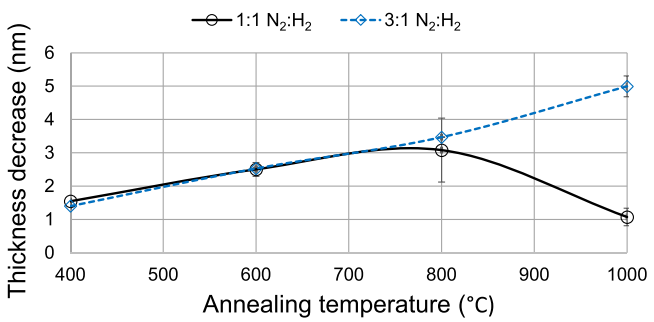

FIG. 3. (Color online) Decrease in the thickness of the AlN films due to annealing treatments. Error bars represent ±1 standard deviation. The 1:1 flow ratio film has the large error at 800 °C.

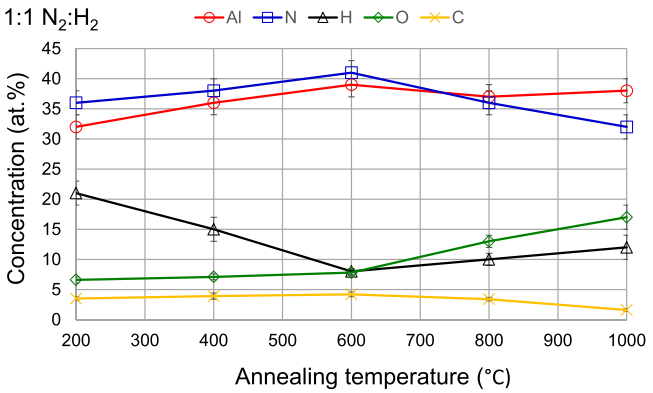

FIG. 4. (Color online) ToF-ERDA elemental composition data of 1:1 N_2:H_2 flow AlN films as a function of annealing temperature.

ToF-ERDA depth profiling (quantitative element concentration), FTIR spectroscopy (qualitative information on chemical constituents), XRD (crystallinity), and HRTEM (crystallinity, crystal size, and homogeneity). Figures 4 and 5 present ToF-ERDA-measured average film compositions of the as-deposited and annealed films. The 200 °C annealing temperature represents the as-deposited state, i.e., the 200 °C thermal treatment is due to the ALD *in situ* temperature. Given error bars are due to the statistics and partly due to the ion-induced losses from the thinnest films during the measurements.

Both films follow similar behavior with respect to the annealing temperature. Clearly, extensive amounts of hydrogen desorption or diffusion into silicon takes place between 400 and 600 °C. The hydrogen that diffuses away from the films could be solute hydrogen in the matrix either in interstitial space or as substitutional atoms in the AlN lattice, in hydroxide compounds, in nonideally reacted TMA ligands or other organic compounds, and any combination of these. TDS is one method to study the desorption kinetics of hydrogen. TDS was utilized here in order to verify hydrogen desorption (Fig. 6). Ramp rate used in the experiment was 6 K/min. The slower ramp rate compared to the HV furnace experiments (16 K/min) may have affected the peak desorption temperature. One example of an in-depth analysis of H desorption and trapping in Al is presented by Young and

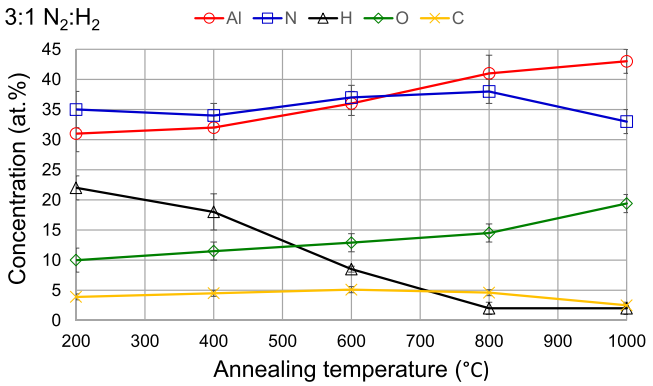

FIG. 5. (Color online) ToF-ERDA elemental composition data of 3:1 N_2:H_2 flow AlN films as a function of annealing temperature.

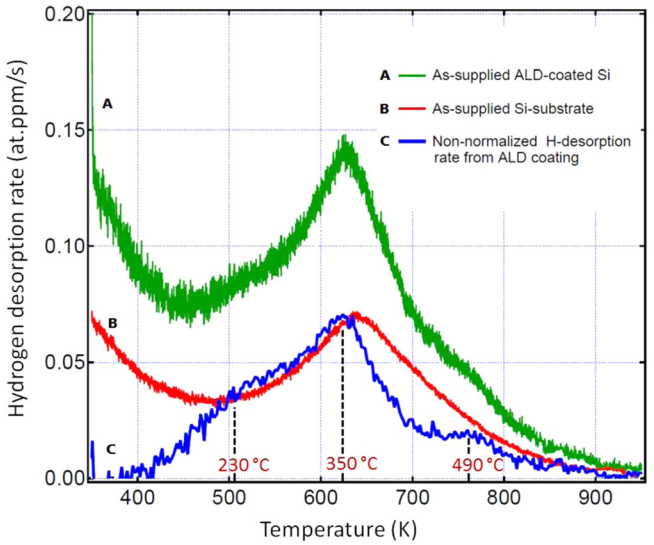

FIG. 6. (Color online) TDS of the 3:1 flow ratio AlN film. TDS measurement indicated that hydrogen is likely embedded in the film in three main species (three bumps in the graph C at approximately 230, 350, and 490 °C). Graph C represents a measurement with subtracted exponential background and Si substrate.

Scully.[34] Different thermal activation energies of different hydrogen species produce desorption rate peaks at different temperatures. Therefore, Fig. 6 would indicate that three main H species exist in the 3:1 flow ratio AlN film. However, AlN deposited on Si may produce also more complicated reaction paths for the hydrogen desorption as there is diffusion into and reaction with the substrate. In order to utilize TDS accurately, it would be advisable to remove the film off the substrate.

After annealing at 600 °C, the hydrogen content and density of the 1:1 N_2:H_2 flow AlN film are at the minimum and the Al:N ratio has approached the 1:1 stoichiometric ratio. Interestingly, there is a slight increase in hydrogen toward 1000 °C annealing. Furthermore, the nitrogen content of the film starts to decrease at and above 800 °C annealing while the amount of oxygen increases. The 3:1 flow samples exhibits similar behavior though the hydrogen content continues to further decrease toward 800 °C annealing. Furthermore, the 3:1 flow samples contain more oxygen in both the as-deposited state, and after 1000 °C annealing compared to the 1:1 flow samples. However, this difference may arise from the surface and the AlN-Si interface oxide. These oxide layers could play a larger role in the total oxide content of the thinner 3:1 flow film. This may also reflect on the density, refractive index, and thickness decrease behavior of the 3:1 film. Nevertheless, the lower initial oxygen in the 1:1 flow samples may originate from the extra hydrogen acting as a getter for the contaminant oxygen in the reactor (the oxidation of AlN is affected by the partial pressures of N_2 and O_2). Similar behavior has been demonstrated for sputtered and CVD AlN.[35,36]

The change in the oxygen content likely reflects also on the density changes of the samples; the 1:1 flow samples have larger changes in the density. The effects on the refractive index are not as pronounced in either of the sample types and the total changes are in the range of a couple percent. Both sample types start to oxidize at approximately 600 °C. It is rather surprising, however, that the transition seems to happen at a rather low temperature since typically the reported temperatures have been over 800 °C depending on the annealing atmosphere. The films are, however, not as dense as bulk AlN and contain impurities which can alter the reactivity of AlN. Moreover, the thermal treatments may render the films more reactive toward the ambient after the annealing. Finally, the amount of carbon impurities decreases most notably after 1000 °C annealing in both sample types.

Figure 7 presents the evolution of the AlN film depth profiles due to the thermal treatments. Only the as-deposited and 1000 °C annealing depth-profiles are presented here since the differences in the depth-profiles are not as marked in the lower temperatures. Most notably, the films contain an oxidized surface and interface after deposition and room temperature storage. After higher temperature (starting at 600 °C) thermal treatments, the films begin to oxidize through the whole thicknesses and the oxygen peak at the surface begins to level out. In addition, the ToF-ERDA data analysis showed an increase in the total amount of oxygen. Therefore, the oxidation must be due to reactions either with ambient oxygen after the thermal treatments or residual oxygen in the HV furnace.

The decrease in the H and C content after annealing happens rather homogeneously and no marked concentration profiles were exhibited by the films. The observations are in agreement with the refractive index and density measurements of the 1:1 flow ratio film, i.e., the films begin to oxidize forming a denser but less polarizable structure. The thickness decrease observation is also in line with this as the thickness decrease is bound to slow as alumina is stable at high temperatures. However, considering the increased amount of hydrogen after 1000 °C annealing hydroxide formation during storage cannot be excluded either. Nevertheless, the unit cell volume for wurtzite AlN is 41.7 $Å^3$, whereas for corundum and bayerite, they are more than 200 $Å^3$ (data retrieved from the ICSD database).[37–39] We propose that the difference in the amount of hydrogen after the 1000 °C annealing and the thickness change in the samples is connected as follows: The 1:1 film has a less stable high temperature composition which ends up forming hydroxide (even below surface) in room temperature storage after the higher temperature annealing. The hydroxide formation will slow down the measured thickness decrease. The 3:1, on the other hand, has a composition more stable in higher temperature (more oxygen) which does not form hydroxide below surface in storage. The continued thickness decrease would then be a consequence of the surface layers slowly evaporating.

The FTIR measurements and analysis were conducted to the two different N_2:H_2 flow ratio sample sets. Figures 8 and 9 present the FTIR transmission spectra of these samples. The proposed IR band assignments are presented in Table I. Two generic observations can be made. First, the valley or peak forms around 2360 cm^{-1}, which are present

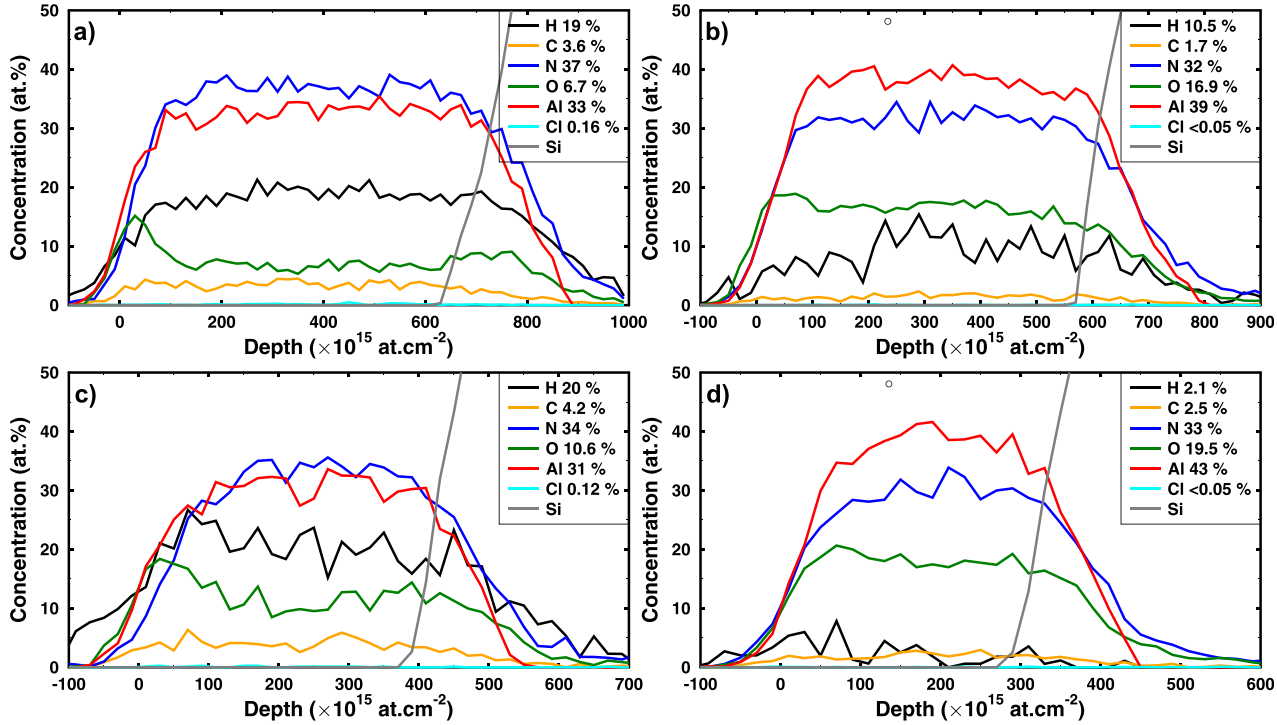

FIG. 7. (Color online) ToF-ERDA depth profiles of AlN films after deposition and annealing at 1000 °C for 1 h. The concentrations of each element were calculated from the midsections of the films. (a) 1:1 N_2:H_2 as-deposited. (b) 1:1 N_2:H_2 annealed at 1000 °C. (c) 3:1 N_2:H_2 as-deposited. (d) 3:1 N_2:H_2 annealed at 1000 °C.

in all of the samples, can be assigned to CO_2 IR absorption and is caused by the deviating CO_2 levels in the measurement chamber.[40] Second, the relatively strong valleys around 1110 cm^{-1} can be credited to Si-O stretching vibrations likely arising from the native oxides of the substrates.[18,41] Also, other interpretations have been given to this band such as the ν(C-N),[22] and the ν(Al-OH),[42] and it is possible that the effect of all three molecules are superimposed to this valley. However, especially the Al-OH is not very likely since O-H group associated absorption is not visible in the higher wavenumbers of 3200 cm^{-1}. It is still noteworthy that the intensity of the 1110 cm^{-1} valley reduces after the annealing at 1000 °C, which could be assigned to thermal decomposition of Si–O bonds. Indeed, according to the standard Gibbs free energy of formation at 1000 °C, the formation of α-Al_2O_3 is almost twice as preferred as the formation of SiO_2 and more than six times favorable than that of AlN.[43]

Both of the N_2:H_2 flow ratio annealing series exhibited similar FTIR spectra. In the low energy end of the spectra, the typical IR phonon modes of AlN are present and in good agreement with the previous research:[44–47] The valleys at 669 and 615 cm^{-1} can be assigned to the E1(TO) and A1(TO) modes, respectively. Moreover, the broad valley at 885 cm^{-1} can be associated with the A1(LO) mode.

The presence of both longitudinal and transverse optical phonon modes can be explained by random bonding of AlN.

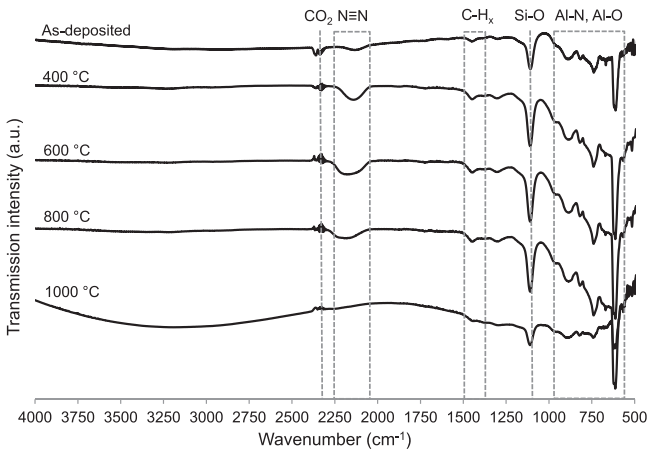

FIG. 8. FTIR transmission spectra for 1:1 N_2:H_2 flow ratio PEALD AlN annealing series.

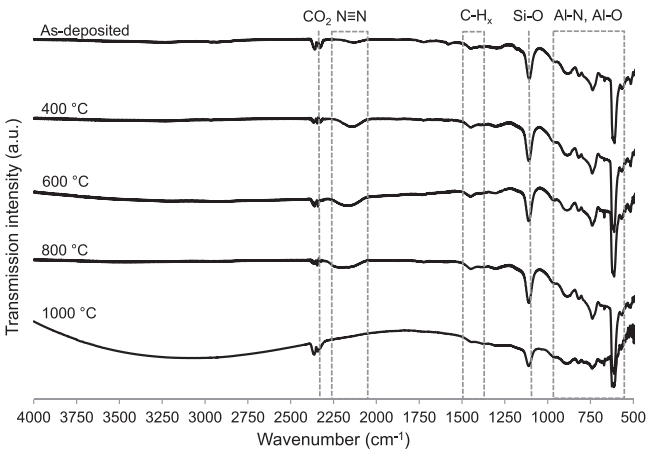

FIG. 9. FTIR transmission spectra for 3:1 N_2:H_2 flow ratio PEALD AlN annealing series.

TABLE I. IR assignments of the identified vibration modes. The stretching and bending modes are denoted ν and δ, respectively. The TO and LO acronyms of Al-N refer to transverse and longitudinal optical phonon modes.

Wave number (cm^{-1})	Vibration mode	Assignment	References
615	A1(TO)	Al–N	44 and 47
669	E1(TO)	Al–N	44 and 47
735	ν(Al–O)	Al–O	18 and 52
885	A1(LO)	Al–N	44–46
960	ν(Al–O)	Al–O	49 and 52
1110	ν(Si–O)	Si–O	18 and 41
1380	δ_s(C–H)	$-CH_3/\equiv CH$	48
1450	δ_a(C–H)	$-CH_3/=CH_2$	22 and 48
2135	ν(N≡N)	$Al-N_2$	28 and 49
2360	$\nu(CO_2)$	CO_2 (gas)	40

However, the A1(TO) seems to be the dominant mode in the spectra. The mode is excited by the electrical field parallel to the wurtzite c-axis [(002) plane]. Therefore, it is possible that the AlN films are preferentially a-plane-oriented. A-plane preferential growth on Si has also been shown with other PEALD AlN.[12,18] It is also possible that the differing AlN mode intensities are caused simply by a higher absorption probability of the A1(TO) mode at 615 cm^{-1}. It is noteworthy that there is no notable evolution in these phonon valleys with respect to annealing below 1000 °C or the N_2:H_2 flow ratios. However, the samples annealed at 1000 °C show clear reduction of the AlN valley intensities. It thus seems that the films maintain their AlN chemical bonding characteristics until annealing at 1000 °C.

The FTIR spectra valleys at 1450 cm^{-1}, and much weaker ones at 1380 cm^{-1}, can be attributed to asymmetric and symmetric bending modes, respectively, of methyl, methylene, and methyne groups.[48] These saturated aliphatic compounds are common impurities in thin films deposited with TMA-based processes.[15] Their existence is supported by the ToF-ERDA data showing clear presence of carbon and hydrogen. Besides these valleys, there is no clear presence of other characteristic aliphatic IR modes between 2800 and 3000 cm^{-1}.[22,48] The characteristic bands do not show alterations with respect to annealing at 800 °C. However, at 1000 °C, the valleys of these groups are significantly reduced in intensity possibly due to outgassing of these groups as gaseous carbohydrates. This is also supported by the ToF-ERDA data which show a clear reduction in carbon atomic concentration. It should be noted that other interpretations have also been given to these modes. Mazur and Cleary[49] contributed the 1446 and 1288 cm^{-1} FTIR peaks to bending modes of N-H complex in NH_3 and NH_4^+ molecules. In the context of this study, this is however less likely since the bending modes of NH molecules are not observed around 3300 cm^{-1}.[22] Previous studies have also proposed that the integrated peak area of this N-H band is proportional to the amount of bonded hydrogen in AlN:H films.[22,50] However, assuming that the hydrogen content would be low due to the lack of hydrogen-related bands can give an erroneous interpretation of the total hydrogen content. Therefore, such conclusion made by Alevli *et al.* based on their x-ray photoelectron spectroscopy and FTIR analysis about their PEALD AlN is questionable.[13]

A broad FTIR valley ranging from 2280 to 2060 cm^{-1} and having the center around 2135 cm^{-1} is present in the samples from the as-deposited to the samples annealed at 800 °C. This mode can be attributed to ν(N≡N) vibrations of the $Al-N_2$ complex.[28,49] The FTIR valleys exhibit a clear shift to higher wavenumbers and broadening as the annealing temperature increases. This applies to both 1:1 and 3:1 flow ratio samples. The shift may be attributed to increased tensile stress in the films but was not measured in this study.[51] The origin of the $Al-N_2$ complex has been demonstrated to be due to N_2H+ ions, originating from N_2:H_2 high density plasma deposition.[28] Remarkably, this valley has completely vanished in the samples annealed at 1000 °C, indicating that the dinitrogen complexes have decomposed entirely. It is likely that these triple nitrogen bonds play a major role in the chemical stability of the films.

Interestingly, in the 1000 °C samples' FTIR data, the disappearance of the ν(N≡N) coincides with the manifestation of a very broad (4000–2000 cm^{-1}) FTIR band with the minimum of the valley at 3200 cm^{-1}. It is thus possible that the decomposing N≡N bonds resulted in N_2 desorption, Al–dangling bonds, and H terminated nitrogen sites.[28] This instead have been reported to make AlN:H thin films more prone to hydrolysis reaction through the ambient air moisture. Hydrolysis leads to the formation of Al-O-OH and/or $Al(OH)_3$ and NH_3, which all are present around the broad band at 3200 cm^{-1}.[28,50] Indeed, the observed decrease in the refractive index, stoichiometry closer to aluminum hydroxide (O/H-ratio of 17/12 at. %), the increased density, and the hindered thickness decrease in the 1000 °C annealed, 1:1 flow ratio sample, all support the claim of higher degree of hydrolysis of the AlN:H compared to the 3:1 sample. The reason why the 3:1 sample showed a minor increase in the refractive index in higher annealing temperatures and continued reduction of thickness could be explained with the higher original oxygen content which stabilized the structure against hydrolysis due to N≡N decomposition.

Additional sources for the oxygen impurities in the PEALD AlN films can include the oxygen impurities during the deposition and the residual oxygen adsorbed during the annealing. Therefore, the deep valley at 735 cm^{-1} in all of the FTIR spectra can be attributed to stretching band of Al-O complex.[18,52] In addition, a much weaker band at 960 cm^{-1} could also be assigned to similar alumina groups.[49,52] However, there is no clear evolvement of these valleys with respect to annealing temperatures or the N_2:H_2 flow ratio alterations except that at 1000 °C the intensity of 735 cm^{-1} valley has diminished. These valleys can be seen as a part of a much broader Al_2O_3 valley that lies approximately between 1000 and 250 cm^{-1}, thus including the AlN phonon modes.[42] It is difficult to determine the exact structure of the AlO_x from this region which has many bands superimposed. Also, the FTIR system utilized could not reach the range 500–250 cm^{-1} where many of the oxide modes have been reported to recede. Still, quite well supported is the presence of alumina transition phases of AlO_6 and AlO_4 stretching

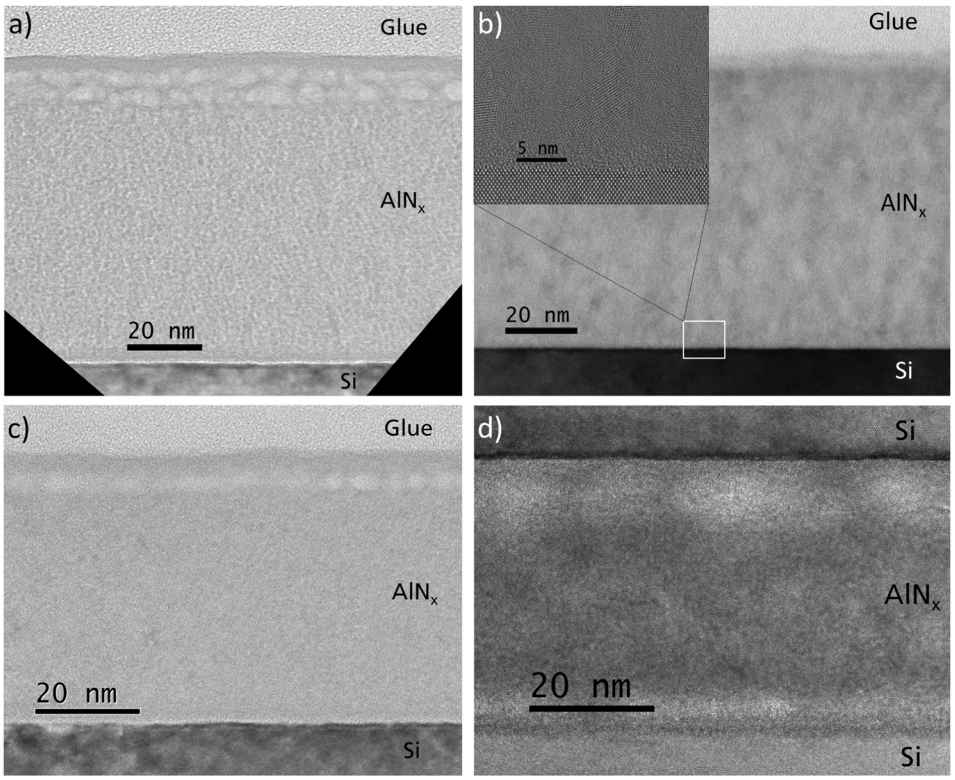

FIG. 10. HRTEM images of the AlN films. (a) 1:1 N_2:H_2 as-deposited. (b) 1:1 N_2:H_2 annealed at 1000 °C. The smallest objective aperture was used in the overview image to maximize the diffraction contrast. A thin amorphous layer exists between the Si and crystallizing film. (c) 3:1 N_2:H_2 as-deposited. (d) 3:1 N_2:H_2 flow sample annealed at 1000 °C (the sample is from a different deposition run and was used in a bonding experiment but is included here to highlight the changes in the micro/nanostructure). The lamella was aligned according to a zone axis of the top Si making the interface at the bottom hazy due to the misalignment between the top and bottom Si.

bands having broad minimum transmission bands around 605 and 800 cm^{-1}.[42]

No XRD peaks were found in the samples. Examining previous studies on PEALD AlN deposited at various temperatures reveals that typically the films are found to be crystalline. More specifically, usually PEALD films with a high Al:N ratio (>0.9) are found to be crystalline,[13–21] whereas AlN films with a low ratio (<0.9) are not found to be crystalline.[15,22] The additional nitrogen beyond the stoichiometric 1:1 ratio can be thought to be an impurity which affects the stability of the amorphous structure. Furthermore, carbon has been shown to affect the crystallinity of other ALD films by stabilizing the amorphous structure, whereas Cl and H content have been shown to have little effect on the crystallinity.[24] However, linking the crystallinity solely to the amount of one element, such as carbon, is not reasonable. For example, crystalline ALD AlN was deposited in the studies of Motamedi and Cadien,[18,19] who also had approximately 3 at. % C (and 9 at. % O), yet their AlN was crystalline. Furthermore, the Al:N ratio in their studies was ~1.5. Indeed, some elements may have a stabilizing effect on the amorphous structures while others can promote crystallization. Such observations have also been made on transition metals by noting that the amorphous structure is stabilized by added impurities such as B, C, N, Si, and P.[53,54] Nevertheless, four TEM samples were imaged to observe the nanostructure of the AlN films and its evolution during annealing treatments. The samples were prepared from the as-deposited films and films annealed at 1000 °C. Especially, the crystallinity and texture of the crystallites were of interest since the XRD analysis was inconclusive but FTIR indicated the films to have a textured nanostructure. Figure 10 presents HRTEM micrographs of the four samples.

The as-deposited films show distinct contrast at the surface due to the oxide-rich layer of the films, i.e., 10–20 nm thick being thicker in the 1:1 samples. The top oxide layer levels out into the films according to the ERDA depth profiles. This manifests as a thinner surface layer in Fig. 10(b). The sample in Fig. 10(d) is not fully comparable but also shows a leveled out contrast at the bond interface (top side). Furthermore, the nanostructure in all of the samples is amorphous in the as-deposited state with little crystallization taking place after annealing at 1000 °C for 1 h. It is noteworthy that during imaging prolonged exposure to the TEM electron beam caused crystallization in the as-deposited samples. Finally, the FFT of Fig. 10(b) was investigated in pursuit of defining the crystal structure. However, no reasonable match was found when comparing the *d* spacings to the most probable compounds (wurtzite and cubic AlN, α-Al_2O_3, and cubic spinel AlON).

IV. SUMMARY AND CONCLUSIONS

AlN films were deposited utilizing PEALD with a TMA, N_2:H_2 process at 200 °C. Two differing flow values were

used for the N_2:H_2 precursor. The resulting AlN films were evaluated in a comparative manner in the as-deposited and vacuum-annealed states. Both of the films had similar characteristics (nanostructure and chemical composition), but exhibited slightly different annealing behavior. However, the observations can be summarized as follows:

(1) The as-deposited films contained up to 20 at. % hydrogen most of which started to effuse during ≥400 °C temperature treatments in high vacuum conditions. Most of the hydrogen in the films was not IR active and did not manifest clearly in the FTIR spectra.
(2) The films began to oxidize after thermal treatments at 600 °C and above. The oxidation behavior was likely affected by the impurities, and chemical bonding state of the impurities in the films.
(3) After annealing at 1000 °C, the dinitrogen triple bonds in the films broke. This caused increased reactivity and thus possible hydrolysis of the films.
(4) The films were amorphous with some crystallization taking place after 1 h annealing at 1000 °C. The crystallinity of the films was affected by the additional N and C impurities in the films which likely stabilized the amorphous structure.
(5) The refractive indices and densities of the films changed, but no straightforward correlation was established between them. The films decreased in thickness by evaporating into the vacuum during annealing.

The purpose of the thermal treatments was to investigate the stability of the PEALD AlN films, deposited at a typical temperature of 200 °C, under elevated temperatures, which could be endured during processes such as bonding, doping activation, and operation in highly demanding environments. The results can also be exploited in improving the quality of the as-deposited films. For example, in order to drive most of the hydrogen out of the films without additional large-scale oxidation of the films, vacuum-annealing at 550–650 °C could be recommended. However, crystallizing the PEALD AlN into polycrystalline hexagonal form, when starting from similar composition as in this study, requires at least an inert, gettering-type, gas environment, such as forming gas (N_2, H_2 mixture). Such gas environment might not be sufficient though as additional hydrolysis may take place after the thermal treatment.

ACKNOWLEDGMENTS

The authors would like to thank Henri Jussila, Elmeri Österlund, Yanling Ge, and Yuriy Yagodzinskyy from Aalto University for the help with the XRD measurements, XRR simulations, TEM imaging, and TDS measurements. The authors are thankful to Andreas Graff from Fraunhofer IMWS for the TEM imaging. Most of the research was conducted at the facilities of Micronova, the Centre for Micro and Nanotechnology. FTIR measurements were conducted at the Nanomicroscopy Center, Aalto University. TEM imaging was conducted at Fraunhofer IMWS.

[1]W. Werdecker and F. Aldinger, IEEE Trans. Compon., Hybrids **7**, 399 (1984).
[2]K. M. Lakin, IEEE Trans. Ultrason. Ferroelectr. **52**, 707 (2005).
[3]S. Strite and H. Morkoç, J. Vac. Sci. Technol., B **10**, 1237 (1992).
[4]K. M. Taylor and C. Lenie, J. Electrochem. Soc. **107**, 308 (1960).
[5]S. Trolier-McKinstry and P. Muralt, J. Electroceram. **12**, 7 (2004).
[6]A. Dadgar, Phys. Status Solidi B **252**, 1063 (2015).
[7]M. Kneissl *et al.*, Semicond. Sci. Technol. **26**, 014035 (2010).
[8]H. Fukuyama, S. Y. Kusunoki, A. Hakomori, and K. Hiraga, J. Appl. Phys. **100**, 024905 (2006).
[9]M. Medraj, Y. Baik, W. T. Thompson, and R. A. L. Drew, J. Mater. Process. Technol. **161**, 415 (2005).
[10]L. Xinjiao, X. Zechuan, H. Ziyou, C. Huazhe, S. Wuda, C. Zhongcai, Z. Feng, and W. Enguang, Thin Solid Films **139**, 261 (1986).
[11]C.-M. Yang, K. Uehara, S.-K. Kim, S. Kameda, H. Nakase, and K. Tsubouchi, IEEE Symp. Ultrasonics **1**, 170 (2003).
[12]M. Alevli, C. Ozgit, I. Donmez, and N. Biyikli, Phys. Status Solidi A **209**, 266 (2012).
[13]M. Alevli, C. Ozgit, I. Donmez, and N. Biyikli, J. Cryst. Growth **335**, 51 (2011).
[14]C. Ozgit-Akgun, E. Goldenberg, A. K. Okyay, and N. Biyikli, J. Mater. Chem. C **2**, 2123 (2014).
[15]M. Bosund, T. Sajavaara, M. Laitinen, T. Huhtio, M. Putkonen, V.-M. Airaksinen, and H. Lipsanen, Appl. Surf. Sci. **257**, 7827 (2011).
[16]H. Van Bui, F. B. Wiggers, A. Gupta, M. D. Nguyen, A. A. I. Aarnink, M. P. de Jong, and A. Y. Kovalgin, J. Vac. Sci. Technol., A **33**, 01A111 (2015).
[17]S. Goerke *et al.*, Appl. Surf. Sci. **338**, 35 (2015).
[18]P. Motamedi and K. Cadien, J. Cryst. Growth **421**, 45 (2015).
[19]P. Motamedi and K. Cadien, Appl. Surf. Sci. **315**, 104 (2014).
[20]N. Nepal, S. B. Qadri, J. K. Hite, N. A. Mahadik, M. A. Mastro, and C. R. Eddy, Jr., Appl. Phys. Lett. **103**, 082110 (2013).
[21]C. Ozgit, I. Donmez, M. Alevli, and N. Biyikli, Thin Solid Films **520**, 2750 (2012).
[22]A. Perros-Pyymaki, H. Hakola, T. Sajavaara, T. Huhtio, and H. Lipsanen, J. Phys. D **46**, 505502 (2013).
[23]H. B. Profijt, S. E. Potts, M. C. M. van de Sanden, and W. M. M. Kessels, J. Vac. Sci. Technol., A **29**, 050801 (2011).
[24]V. Miikkulainen, M. Leskelä, M. Ritala, and R. L. Puurunen, J. Appl. Phys. **113**, 021301 (2013).
[25]C.-Y. Lin and F.-H. Lu, J. Eur. Ceram. Soc. **28**, 691 (2008).
[26]F. Ansart, H. Ganda, R. Saporte, and J. P. Traverse, Thin Solid Films **260**, 38 (1995).
[27]R. Dalmau, R. Collazo, S. Mita, and Z. Sitar, J. Electron. Mater. **36**, 414 (2007).
[28]X.-D. Wang, K. W. Hipps, and U. Mazur, Langmuir **8**, 1347 (1992).
[29]J. Tiilikainen, J. M. Tilli, V. Bosund, M. Mattila, T. Hakkarainen, V.-M. Airaksinen, and H. Lipsanen, J. Phys. D: Appl. Phys. **40**, 215 (2007).
[30]M. Laitinen, M. Rossi, J. Julin, and T. Sajavaara, Nucl. Instrum. Methods B **337**, 55 (2014).
[31]O. Todoshchebko, "Hydrogen effects on austenitic stainless steels and high-strength carbon steels," Doctoral dissertation (Aalto University, 2015).
[32]Ioffe Institute, "New semiconductor materials, characteristics and properties," http://www.ioffe.ru/SVA/NSM/Semicond/AlN/basic.html, accessed 12 April 2016.
[33]R. E. Newnham, *Properties of Materials: Anisotropy, Symmetry, Structure* (Oxford University, New York, 2004), p. 280.
[34]G. A. Young and J. R. Scully, Acta Mater. **46**, 6337 (1998).
[35]Y.-J. Yong and J.-Y. Lee, J. Vac. Sci. Technol., A **15**, 390 (1997).
[36]F. Hasegawa, T. Takahashi, K. Kubo, and Y. Nannichi, Jpn. J. Appl. Phys., Part 1 **26**, 1555 (1987).
[37]R. Rothbauer and F. Zigan, Z. Kristallogr. **125**, 317 (1967).
[38]H. Schulz and K. H. Thiemann, Solid State Commun. **23**, 815 (1977).
[39]D. E. Cox, A. R. Moodenbaugh, A. W. Sleight, and H. Y. Chen, NIST Spec. Publ. **567**, 189 (1979).
[40]M.-I. Baraton, X. Chen, and K. E. Gonsalves, Nanostruct. Mater. **8**, 435 (1997).
[41]R. Tian, O. Seitz, M. Li, W. Hu, Y. J. Chabal, and J. Gao, Langmuir **26**, 4563 (2010).
[42]A. Boumaza, L. Favaro, J. Lédion, G. Sattonnay, J. B. Brubach, P. Berthet, A. M. Huntz, P. Roy, and R. Tétot, J. Solid State Chem. **182**, 1171 (2009).
[43]M. W. Chase, *NIST-JANAF Thermochemical Tables*, 4th ed. (American Institute of Physics, Woodbury, NY, 1998).

[44]C. Bungaro, K. Rapcewicz, and J. Bernholc, Phys. Rev. B **61**, 6720 (2000).
[45]M. D. Sciacca, A. J. Mayur, E. Oh, A. K. Ramdas, S. Rodriguez, J. K. Furdyna, M. R. Melloch, C. P. Beetz, and W. S. Yoo, Phys. Rev. B **51**, 7744 (1995).
[46]S. Kuchibhatla, L. E. Rodak, and D. Korakakis, Thin Solid Films **519**, 117 (2010).
[47]S. Sanz-Hervas, E. Iborra, M. Clement, J. Sangrador, and M. Aguilar, Diamond Relat. Mater. **12**, 1186 (2003).
[48]J. Coates, *Interpretation of Infrared Spectra, A Practical Approach*, Encyclopedia of Analytical Chemistry (Wiley, Chichester, 2000).
[49]U. Mazur and A. C. Cleary, J. Phys. Chem. **94**, 189 (1990).
[50]M.-H. Cho, Y.-S. Kang, H.-Y. Kim, P. S. Lee, and J.-Y. Lee, Electrochem. Solid State **4**, F7 (2001).
[51]J. X. Zhang, H. Cheng, Y. Z. Chen, A. Uddin, S. Yuan, S. J. Geng, and S. Zhang, Surf. Coat. Technol. **198**, 68 (2005).
[52]A. Raveh, Z. K. Tsameret, and E. Grossman, Surf. Coat. Technol. **88**, 103 (1996).
[53]T. Laurila, "Tantalum-based diffusion barriers for copper metallization," Doctoral dissertation (Helsinki University of Technology, 2001).
[54]M. A. Nicolet, *Diffusion in Amorphous Materials*, edited by H. Jain and D. Gupta (TMS, Warrendale, 1994), pp. 225–234.